

JefiPIC: A 3-D Particle-in-Cell Method Based on Jefimenko's Equations on GPU

Jiannan Chen¹, Junjie Zhang^{1,*}, Xueming Li², Yongtao Zhao³

1. Northwest Institute of Nuclear Technology, Xi'an, 710024, China
2. Institute of Applied Physics and Computational Mathematics, Beijing, 100094, China
3. MOE Key Laboratory for Nonequilibrium Synthesis and Modulation of Condensed Matter, School of Science, Xi'an Jiaotong University, Xi'an, 710049, China

* Corresponding to Email: zjacob@mail.ustc.edu.cn

Abstract: In this paper, we have proposed a new 3-D particle-in-cell (PIC) code which employs the integral Jefimenko's equations as the electromagnetic field solver. The challenging task is made possible with the help of the state-of-the-art graphic processing units (GPU) apparatus. To match the location of the fields and current densities defined in Jefimenko's equations, we have modified the field and charge interpolation methods. Different from the classical finite-difference time-domain (FDTD) method, the integral equations do not require strict charge conservation approaches during the particle emission moments. Our proposed method can naturally deal with the electrostatic problem, and does not need to deal with the boundary conditions, which is appropriate in solving open boundary plasma systems. To verify our code, we compare the particle evolution of a pure electron system simulated by two other codes: one is an open-source 3-Dimensional (3-D) PIC code based on FDTD, and the other is a 3-D numerical Boltzmann equations solver using Jefimenko's equations. The numerical results imply that it is beneficial to combine the time consuming Jefimenko's equations and the PIC method to provide accurate electromagnetic fields and particle distributions in describing open-boundary plasma systems. Our verification demonstrates that we can accomplish such task within an acceptable execution time with the use of the GPU.

Keywords: particle-in-cell, finite-difference time-domain, Jefimenko's equation, interpolation method, GPU

1 Introduction

1.1 Background

Particle-in-cell (PIC), a method that adopts the concept of macro-particles to describe the particle in similar phase space states, was first put forward by Dawson for studying the Langmuir wave in 1-D electrostatic plasma in the 1960s [1]. Later, Langdon and Birdsall modified the PIC model to the finite-size particle [2] or particle cloud [3], and solved the problem of the Coulomb collision between particles. Further, Marder [4] and Villasenor [5] amended the error of the electric field divergence, and Birdsall [6] and Vahedi [7] introduced the Monte Carlo collision into PIC, which made PIC step into the practical application. Nowadays, PIC is often used to simulate the controlled/laser thermonuclear fusion [8], [9], nuclear explosion effects [10], [11], [12], space physics [13], or design the vacuum electronic devices [14], [15], [16].

The PIC method provides an intuitive description of the motion of charged particles, and it is more accessible for researchers to analyze the data. Under this condition, many mature commercial software and open-source PIC codes have shown up, for example, MAGIC [17] XOOPIIC [18], ICEPIC [19], UNIPIC [20], freely available EPOCH [21], [22] and so on.

On the whole, the PIC model includes two important parts. One is to update the dynamics of electromagnetic (EM) fields from Maxwell's equations,

$$\varepsilon \frac{\partial \mathbf{E}}{\partial t} = \nabla \times \frac{\mathbf{B}}{\mu} - \mathbf{J}, \quad (1)$$

$$\frac{\partial \mathbf{B}}{\partial t} = -\nabla \times \mathbf{E}, \quad (2)$$

$$\nabla \cdot \mathbf{E} = \frac{\rho}{\epsilon}, \quad (3)$$

$$\nabla \cdot \mathbf{B} = 0, \quad (4)$$

where \mathbf{E} and \mathbf{B} are the electric and magnetic fields, ϵ and μ are the permittivity and permeability of the medium, ρ and \mathbf{J} are the electric density and electric current density.

The other part is to update and follow the positions and velocities of the charged particles by the Newton–Lorentz force equations of motion

$$\frac{d}{dt} \gamma m \mathbf{v} = q(\mathbf{E} + \mathbf{v} \times \mathbf{B}), \quad (5)$$

$$\frac{d}{dt} \mathbf{r} = \mathbf{v}, \quad (6)$$

where m , q , \mathbf{r} , and \mathbf{v} are the mass, charge, displacement, and velocity of the particle, respectively. The relativistic factor is

$$\gamma = \frac{1}{\sqrt{1 - (v/c)^2}} = \sqrt{1 + (u/c)^2}, \quad (7)$$

where c is the speed of light, $\mathbf{u} = \gamma \mathbf{v}$. The current continuity equation is satisfied

$$\frac{\partial \rho}{\partial t} + \nabla \cdot \mathbf{J} = 0. \quad (8)$$

As a result, to solve the Maxwell's equations, we only need to consider the first two curl equations Eqs. (1) ~ (2) as well as the current continuity equation Eq. (8). The rest two divergence equations Eqs. (3) ~ (4) can be obtained accordingly.

The usual method for solving Eqs. (1) ~ (2) in PIC is the FDTD method [23], which is born naturally to solve the curl equations due to its sparsity and simplicity compared with other methods, such as the finite element method [24], [25] which needs to solve a complex matrix. Meanwhile, due to Eq. (8), once an electron is produced, there will generate certain electric fields acting as positive particles deposit where the electron emits. We name the positive particle after “invented positive charge”, of which the charge is changeable according to the field interpolation method [26], [27], [28]. Some field interpolation methods make the charge of the “invented positive charge” just reverse to that of the emission electron, which are called the charge conservation interpolation methods.

1.2 Motivation

The description of plasma systems in terms of the FDTD-based PIC simulation requires elaborate algorithms to handle the propagation of the EM fields. The scenario can be simplified if one adopts the integral equations such as the Jefimenko's equations [29], [30]. However, known as the general solutions of the Maxwell's equations, Jefimenko's equations are resource-consuming, especially when combined with the PIC methods.

In this paper, we have proposed a Jefimenko-based PIC method named JefiPIC, which employs the Jefimenko's equations to provide the EM fields in the PIC simulation. The challenging task is made possible on the GPU device. As long as given the initial condition of the charged particles and the background EM fields, our code will automatically compute the space-time distribution of the source terms ρ and \mathbf{J} , as well as the evolution of the plasma. Our method is beneficial in describing the plasma systems

with open physical boundaries, such as the space plasma [31], quark gluon plasma [32] or high-altitude nuclear explosion [33], [34], which are not designed to deal with interaction of fields and the complicated geometrical objects [35].

Compared with the current FDTD-based PIC simulation, JefiPIC has certain benefits. First, one needs to employ proper boundary conditions [36], [37] to cut off and then absorb the EM fields in the FDTD method. The numerical results via the FDTD method are sensitive to the choice of the boundary conditions. Minor errors in the potential reflected waves would raise large errors to the whole plasma system. Since we do not need to set the boundaries conditions in JefiPIC, our method is physically and algorithmically simpler in describing open plasma systems. Second, JefiPIC can naturally mimic the evolution of low frequency plasmas. It is reported that the FDTD method encounters difficulties in describing low frequency EM effects [38][39], hence we usually use the electrostatic Poisson's equation [14] as a better option in the PIC model. Third, as mentioned above, the FDTD-based PIC comes up with undesired charge conservation errors to deal with the particle emission, depending on the field interpolations methods. JefiPIC, on the other hand, does not encounter such numerical difficulties. Fourthly, the conservation of charge law will also lead to a problem when we want to simulate a pure electric system in the free space. In such condition, we need to assume that the initial electrons have already spread their fields to infinity to amend the electric field divergence. If the electron emission is continuously carried out during the computation, the amendments should be adopted at each time step. In JefiPIC, we do not encounter such challenge.

However, the numerical simulation of Jefimenko's equations is extremely time consuming, since the integral is performed over the entire source volume with retarded time. For a performance enhancement, we use the GPU-based package JefiGPU [40]. JefiGPU performs the Jefimenko's equation directly on GPU with the help of the high dimensional integration package ZMCintegral [41]. With the utilization of JefiGPU, we can perform the evolution of the plasma systems within an acceptable execution time. Meanwhile, we also implement the particle motion equations on GPU, so that the proposed JefiPIC is a fully GPU-based plasma simulator. All quantities are consistently defined on the GPU memory which guarantees a fast execution.

The paper is organized as follows. In Sec. 2 we show the detailed designing process of our proposed JefiPIC method, including the interpolation method of particles and fields and the Jefimenko's equations. In Sec. 3, we compare the results from JefiPIC, EPOCH and RBG-Maxwell [32], [42] by modeling a pure electron system, and analyze the advantages of JefiPIC. In Sec. 4, we conclude the work and discuss the future research direction.

2 Method

2.1 Jefimenko's equation

As mentioned before, the EM fields in JefiPIC are obtained by the Jefimenko's equations

$$\mathbf{E}(\mathbf{r}, t) = \frac{1}{4\pi\epsilon_0} \int \left[\frac{\mathbf{r} - \mathbf{r}'}{|\mathbf{r} - \mathbf{r}'|^3} \rho(\mathbf{r}', t_r) + \frac{\mathbf{r} - \mathbf{r}'}{|\mathbf{r} - \mathbf{r}'|^2} \frac{1}{c} \frac{\partial \rho(\mathbf{r}', t_r)}{\partial t} - \frac{1}{|\mathbf{r} - \mathbf{r}'|} \frac{1}{c^2} \frac{\partial \mathbf{J}(\mathbf{r}', t_r)}{\partial t} \right] d^3 \mathbf{r}', \quad (9)$$

$$\mathbf{B}(\mathbf{r}, t) = -\frac{1}{4\pi} \int \left[\frac{\mathbf{r} - \mathbf{r}'}{|\mathbf{r} - \mathbf{r}'|^3} \times \mathbf{J}(\mathbf{r}', t_r) + \frac{\mathbf{r} - \mathbf{r}'}{|\mathbf{r} - \mathbf{r}'|^2} \times \frac{1}{c} \frac{\partial \mathbf{J}(\mathbf{r}', t_r)}{\partial t} \right] d^3 \mathbf{r}', \quad (10)$$

$$t_r = t - |\mathbf{r} - \mathbf{r}'|, \quad (11)$$

where t_r is the retarded time, and (\mathbf{r}, t) represents the space-time point. \mathbf{r} and \mathbf{r}' refer to the displacements in the observation and source region as the form of (x, y, z) and (x', y', z') . Given the current density \mathbf{J} and charge density ρ in the space-time, the EM fields at point \mathbf{r} can be calculated via Eqs. (9) ~ (11). Once

obtained the EM fields, the particles are easily pushed according to the Newton–Lorentz functions Eqs. (5) ~ (6).

In JefiPIC, we divide the source region and observation region with the same cuboid grids for numerical computation. Under this condition, Eqs. (9) ~ (11) are discretized as

$$\mathbf{E}(\mathbf{r}, t) = \frac{dx'dy'dz'}{4\pi\epsilon_0} \sum_{i,j,k} \left[\frac{\mathbf{r} - \mathbf{r}'_{i,j,k}}{|\mathbf{r} - \mathbf{r}'_{i,j,k}|^3} \rho(\mathbf{r}'_{i,j,k}, t_r) \right. \\ \left. + \frac{\mathbf{r} - \mathbf{r}'_{i,j,k}}{|\mathbf{r} - \mathbf{r}'_{i,j,k}|^2} \frac{1}{c} \frac{\rho(\mathbf{r}'_{i,j,k}, t_r) - \rho(\mathbf{r}'_{i,j,k}, t_r - dt)}{dt} \right. \\ \left. - \frac{1}{|\mathbf{r} - \mathbf{r}'_{i,j,k}|} \frac{1}{c^2} \frac{\mathbf{J}(\mathbf{r}'_{i,j,k}, t_r) - \mathbf{J}(\mathbf{r}'_{i,j,k}, t_r - dt)}{dt} \right], \quad (12)$$

$$\mathbf{B}(\mathbf{r}, t) = -\frac{dx'dy'dz'}{4\pi} \sum_{i,j,k} \left[\frac{\mathbf{r} - \mathbf{r}'_{i,j,k}}{|\mathbf{r} - \mathbf{r}'_{i,j,k}|^3} \times \mathbf{J}(\mathbf{r}'_{i,j,k}, t_r) \right. \\ \left. + \frac{\mathbf{r} - \mathbf{r}'_{i,j,k}}{|\mathbf{r} - \mathbf{r}'_{i,j,k}|^2} \times \frac{1}{c} \frac{\mathbf{J}(\mathbf{r}'_{i,j,k}, t_r) - \mathbf{J}(\mathbf{r}'_{i,j,k}, t_r - dt)}{dt} \right], \quad (13)$$

$$t_r = t - |\mathbf{r} - \mathbf{r}'_{i,j,k}|, \quad (14)$$

where the indices i, j , and k denote the index of the grids in the source region. The numerical value for $\mathbf{r}'_{i,j,k}$ is simply the coordinate at the center of the grid, and dx' , dy' , and dz' are the sizes of the grid in the source region. For computational convenience, \mathbf{J} , ρ , \mathbf{E} and \mathbf{B} are all defined at the center of the grids.

2.2 Particle moving

The Newton–Lorentz force equations are discretized by the central leap-frog difference method as

$$\frac{\gamma m(\mathbf{v}^{n+1/2} - \mathbf{v}^{n-1/2})}{dt} = q \left(\mathbf{E}^n + \frac{\mathbf{v}^{n+1/2} + \mathbf{v}^{n-1/2}}{2} \times \mathbf{B}^n \right), \quad (15)$$

$$\frac{\mathbf{r}^{n+1} - \mathbf{r}^n}{dt} = \mathbf{v}^{n+1/2}, \quad (16)$$

where the superscript n denotes the n^{th} time step in simulation. However, the advancement of velocity is an implicit equation which is tough to solve directly. So, the Boris particle pusher is employed, and Eq. (15) is separated into three steps as

$$\mathbf{v}^- = \mathbf{v}^{n-1/2} + \frac{q\mathbf{E}^n}{m} \frac{dt}{2}, \quad (17)$$

$$\frac{(\mathbf{v}^+ + \mathbf{v}^-)}{dt} = \frac{q}{2\gamma m} (\mathbf{v}^+ + \mathbf{v}^-) \times \mathbf{B}^n, \quad (18)$$

$$\mathbf{v}^{n+1/2} = \mathbf{v}^+ + \frac{q\mathbf{E}^n}{m} \frac{dt}{2}. \quad (19)$$

2.3 Charge and field interpolation method

Since the electromagnetic fields, currents, and charge densities need to be allocated at the center of the grids in Jefimenko's equations which is different from that in FDTD, we should modify the field and particle interpolation methods. The traditional PIC methods usually adopt two interpolation methods. One is the so-called charge conservation method, while it will bring numerical noises inevitably. The other is the linear interpolation method with first-order accuracy causing less noises. However, the latter one breaks the charge conservation law. In fact, some researchers employ higher accuracy interpolation methods such as Lagrange interpolation or spline interpolation, but the complexity and more time-consuming limit their application.

Because of the difference between integral equations and difference equations, JefiPIC does not face the charge conservation problem. Hence, we use the first-order linear interpolation method, which has acceptable numerical noises and computational time.

In the 3-D model, linear interpolation is regarded as the volume-weighted interpolation. For convenience, we use a 2-D model, which utilizes the first-order area-weighted interpolation, to explain how the particle interpolation works in Figure 1. Assuming that there is one particle in some source region, labeled by a “star”, the charge of this particle should be allocated to its nearest center nodes indicated by the solid points. In a 3-D model, one particle should be allocated to 8 nodes, while in a 2-D model there are only 4 nodes with indices (i, j) , $(i+1, j)$, $(i, j+1)$ and $(i+1, j+1)$. According to the area-weighted interpolation method, the allocated charge on one node is equal to the charge of the particle times the weight, which is ratio of the shaded area of its thither corresponding rectangle to the area of one grid.

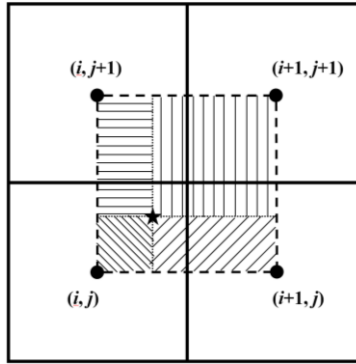


Figure 1. Area-weighted interpolation. The particle is indicated by a “star” and is interpolated to the four neighbor grids according to the ratio of the corresponding shaded area to the grid area.

Since the variables are defined at the center of the grids, we firstly find the indices of the nodes

$$i = \left[\frac{x - 0.5 \cdot dx'}{dx'} \right], \quad j = \left[\frac{y - 0.5 \cdot dy'}{dy'} \right], \quad k = \left[\frac{z - 0.5 \cdot dz'}{dz'} \right] \quad (20)$$

Following the first-order volume-weighted interpolation method, particles with index (i, j, k) should be interpolated to the adjacent grids. Thus, the charge densities on the nearest nodes are expressed as

$$\rho_{i,j,k} = (1 - \alpha)(1 - \beta)(1 - \chi)\rho, \quad (21)$$

$$\rho_{i+1,j,k} = \alpha(1 - \beta)(1 - \chi)\rho, \quad (22)$$

$$\rho_{i,j+1,k} = (1 - \alpha)\beta(1 - \chi)\rho, \quad (23)$$

$$\rho_{i,j,k+1} = (1 - \alpha)(1 - \beta)\chi\rho, \quad (24)$$

$$\rho_{i+1,j+1,k} = \alpha\beta(1-\chi)\rho, \quad (25)$$

$$\rho_{i+1,j,k+1} = \alpha(1-\beta)\chi\rho, \quad (26)$$

$$\rho_{i,j+1,k+1} = (1-\alpha)\beta\chi\rho, \quad (27)$$

$$\rho_{i+1,j+1,k+1} = \alpha\beta\chi\rho, \quad (28)$$

where

$$\alpha = \frac{x - i \cdot dx'}{dx'}, \quad \beta = \frac{y - j \cdot dy'}{dy'}, \quad \chi = \frac{z - k \cdot dz'}{dz'}, \quad (29)$$

$$\rho = \frac{q}{dx' dy' dz'}, \quad (30)$$

and q is the charge of the moving particle. The current densities can be easily obtained by two steps. One is to multiply the charge of the particle by its velocities in three directions, and the second step is to interpolate the product to the neighbor grids. However, there is one thing to notice that the number of the adjacent nodes will change if the particles arrive at the grid boundary. In the implementation, if the distance between a particle and any boundary is less than a half grid, for instance, $x < 0.5 \cdot dx$, or $x > (i+0.5) \cdot dx$, we will denote it as a boundary particle. When the particles stay at the boundary face or boundary edge, the charge will be allocated on 4 or 2 adjacent nodes, respectively. When it comes to the boundary corner, only the corner grid will be allocated.

The field interpolation has a reverse execution process to the charge interpolation method. The EM fields acting on a certain particle are interpolated by the weighted summation of the EM fields in the adjacent grids. Thus, the electric field on a particle in grid (i, j, k) can be evaluated as

$$\begin{aligned} \mathbf{E}_{i,j,k}^q = & (1-\alpha)(1-\beta)(1-\chi)\mathbf{E}_{i,j,k} + \alpha(1-\beta)(1-\chi)\mathbf{E}_{i+1,j,k} \\ & + (1-\alpha)\beta(1-\chi)\mathbf{E}_{i,j+1,k} + (1-\alpha)(1-\beta)\chi\mathbf{E}_{i,j,k+1} \\ & + \alpha\beta(1-\chi)\mathbf{E}_{i+1,j+1,k} + \alpha(1-\beta)\chi\mathbf{E}_{i+1,j,k+1} \\ & + (1-\alpha)\beta\chi\mathbf{E}_{i,j+1,k+1} + \alpha\beta\chi\mathbf{E}_{i+1,j+1,k+1} \end{aligned} \quad (31)$$

The parameters in Eq. (31) are the same as those in Eq. (29). One can obtain the magnetic field on the particle accordingly. Note that the number of the adjacent nodes which participate in pushing the particle obeys the same rule in the particle interpolation.

3 Computational Model and Result

To verify our code JefiPIC, we use other two codes for comparison. One is an open-source 3-D PIC code EPOCH and the other is a 3-D plasma simulator RGB-Maxwell. Since the numerical values for physical quantities must be within the range of machine precision, i.e., float64, we need to convert the quantities from International Unit of System (SI) to a new unit system. In this paper, we use the Flexible Unit (FU) as in RBG-Maxwell (see appendix for a short introduction of FU). By choosing proper values for vacuum permittivity ϵ_0 , reduced Planck constant \hbar , speed of light c and λ which relates the energy in SI and FU, we can limit most of the numerical values in machine precision. **Note that the use of FU does not change the physics of the plasma system.**

In the three codes, we divide the computational region with the same spatial grid size $dx = dy = dz =$

10^{-5} m. The total computational time is 10^{-9} s. In EPOCH, owing to using the difference method, the time step dt needs to satisfy the CFL condition [43] which limits the time step according to the grid sizes

$$c \cdot dt \leq \frac{1}{\sqrt{\frac{1}{(dx)^2} + \frac{1}{(dy)^2} + \frac{1}{(dz)^2}}}, \quad (32)$$

JefiPIC and RGB-Maxwell utilize Jefimenko's equation instead, so there is little limit to the time step. However, in order to gain a more accurate result, we set the time step $dt = 10^{-13}$ s with 10000 time steps.

In our simulation, we set 1 grid in x -direction, 251 grids in y -direction, and 111 grids in z -direction in JefiPIC and RGB-Maxwell, but 3 grids in x -direction in EPOCH (as the request of its high-order interpolation method). At the beginning, a batch of free electrons are uniformly placed in a strip of grids where $y = 10 \cdot dy$, z is from $6 \cdot dz$ to $106 \cdot dz$ ($x = 2 \cdot dx$ in EPOCH, the middle layer long x -axis) as shown in Figure 2.

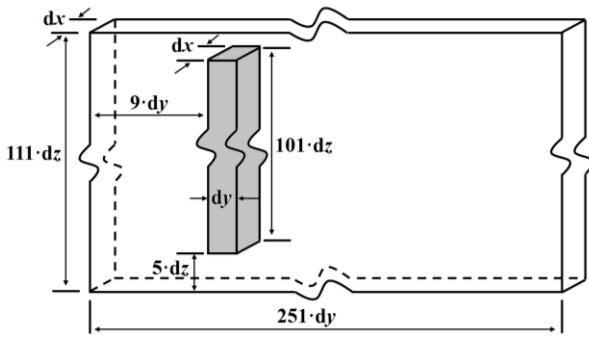


Figure 2. The initial electron distribution in the simulation. The total computational space is of size $1 \cdot dx \times 251 \cdot dy \times 111 \cdot dz$. The particles are placed in the shaded region.

The electrons are emitted with velocity only in the y -direction with initial energy 10 eV. We restrict the transverse motions of the electrons in the XOZ plane by posing a constant magnetic field $B = 10$ T along the y -direction. The total initial charge is 5×10^{-14} C with electron number 3.125×10^5 . In JefiPIC, each particle is tracked in a CUDA kernel. Since the maximum number of CUDA kernels are around 10^9 on one A100 GPU card, we can simulate at most 10^9 particles at the same time in JefiPIC. Thus, in order to decrease the numerical noise, we use one macro-particle standing for a hundredth electron, and thus there are 3.125×10^7 particles in our simulation. In EPOCH, the code dynamically adjusts the weight of the particles so that the particle number in per grid is around 100. In RGB-Maxwell, the initial condition is a distribution function defined on the six-dimensional phase space.

Figure 3 shows the particle distribution by the three codes at different time snapshots. As we can see, the overall distributions are similar that the particles locate almost the same regions at each time. The particles are repelled from each other in the y -direction and limited in the XOZ plane by the external magnetic field. Meanwhile, results given by JefiPIC and RBG-Maxwell are more similar. Since RGB-Maxwell solves the Boltzmann equations directly, which is already the ensemble averaged result, its particle distributions are smoother compared with that of JefiPIC, in which we may observe a clearer and denser layer in the central electron distribution. The densest region of the particle distribution of the two integral-equation-based codes locates at the two ends of the electron bar, while that of EPOCH locates in the center part. Meanwhile, EPOCH causes less particle repulsion compared with the other two codes. However, the distribution from EPOCH is reasonable. Since EPOCH utilizes the FDTD method, which is weak at computing the electrostatic problems. Meanwhile, on account of the effect of both the “invented positive charge” and the field and particle interpolation method, undesired edge effect is observed. The

charge conservation law is kept until parts of the particles reach the right boundary.

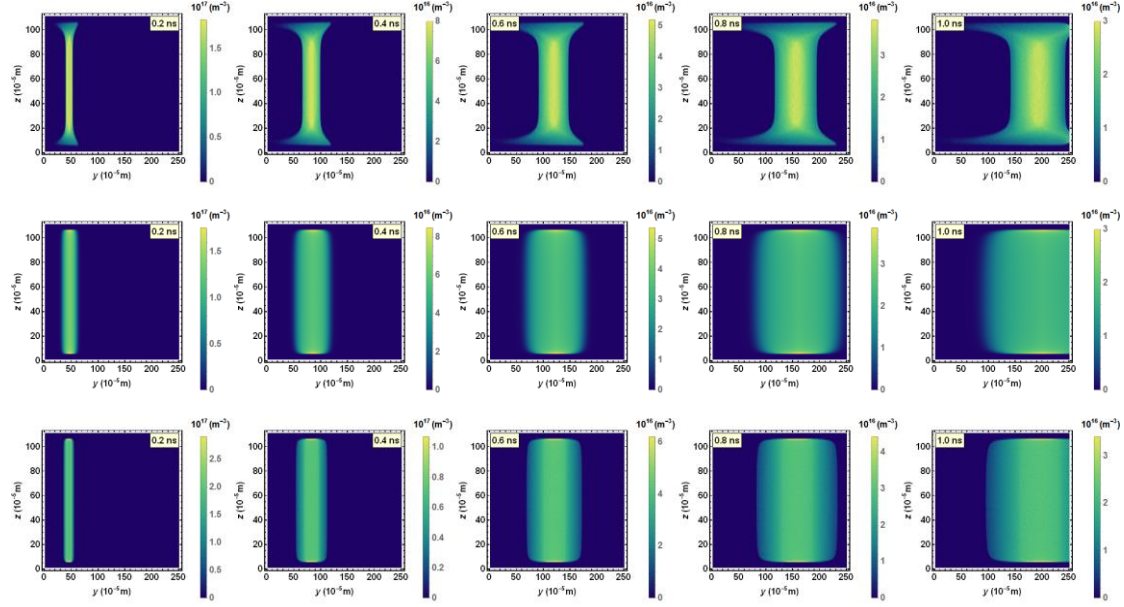


Figure 3. Particle distribution in the YOZ plane. (a) is the result from EPOCH in the $x=1 \cdot \text{dx}$ plane, (b) is from RGB-Maxwell, and (c) is from JefiPIC. The time snapshots are chosen to be $t = 0.2, 0.4, 0.6, 0.8$ and 1.0 ns.

Figure 4 shows the electron number density along y -axis where the grid index of the x and z -axes are kept fixed (here, we choose $k = 55$, $i = 2$ in EPOCH and $i = 1$ in the other two codes). It is shown in Figure 3(a) that EPOCH allocates the electron number density or charge density more uniformly than the others. The electron density is higher at the center in EPOCH at later times though it starts with a lower density. After diagnosing the particle distribution, we find that as time passes by, the particle interpolation of EPOCH makes the number density larger in the center while smaller in the edge, while the total charge is conserved all the time.

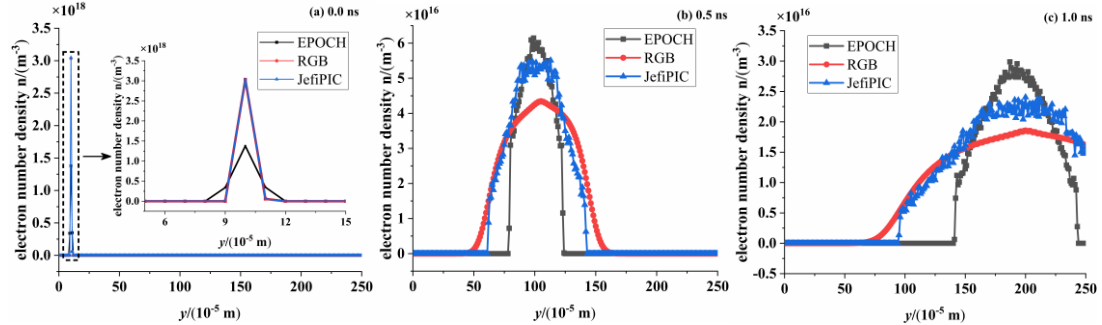


Figure 4. The electron number density along y -axis. The grid index of the x and z -axes are kept fixed with $k = 55$, $i = 2$ in EPOCH and $i = 1$ in the other two codes.

We further diagnose the electric field in grid with index $(i = 2, j = 50, k = 55)$ in EPOCH and at point $(i = 1, j = 50, k = 55)$ in RGB-Maxwell and JefiPIC. The results are displayed in Figure 5. With the same EM solver, JefiPIC and RGB-Maxwell give the similar waveforms of the electric field according to the electron density shown in Figure 4. For EPOCH, lack of the ability to calculate electrostatic or low-frequency projects, the densest electron density gives the lowest electric field peak value on the contrary. This shortcoming also leads to that the electric fields are produced only when the particles pass by the diagnose point. However, the peak times match with one another, indicating that the particle motions are similar.

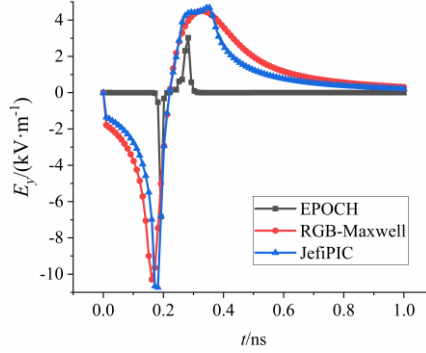


Figure 5. The electric fields obtained in grid with index ($i = 2, j = 50, k = 55$) in EPOCH and point ($i = 1, j = 50, k = 55$) in RGB-Maxwell and JefiPIC. The black squares, red circles and blue triangles indicate the result from EPOCH, RGB-Maxwell and JefiPIC.

As mentioned above, by using the GPU, the execution time of JefiGPU is acceptable, which is of the same order as the others, shown in Table I. We think that EPOCH behaves worse just because of the more grids it needs to handle. Meanwhile, we also test the time consumption of JefiGPU with the increasing of the macro-particle numbers. It can be seen from Fig. 6 that as long as the particle number is less than one percent of the limitation of CUDA kernel (\sim a bit less than 10^7), the computational time changes little. This is due to the high degree of parallelism on GPU and less data transferring between CPU and GPU. However, once the particle number is beyond 10^7 , the time cost will be multiplying. Note that if the allocated kernel number (i.e., the particle number in JefiGPU) exceeds the limitation by CUDA ($\sim 10^9$), the computed result will be incorrect. Fortunately, $10^7\sim 10^8$ macro-particles are quite enough for the usual simulation with controlled noises.

Table I. The computational time of the three codes

Code	EPOCH	RGB-Maxwell	JefiPIC
Time cost	~ 1 h	~ 0.8 h	~ 0.6 h
Device info	Intel Xeon Gold 6132	Tesla A100	Tesla A100

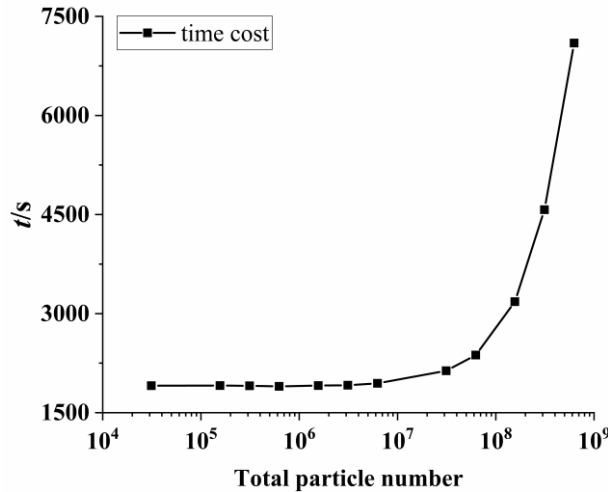


Figure 6. The time cost of JefiPIC with different particle numbers. Enslaved to the CUDA kernel, the upper limit of the particle number is around 10^9 .

4 Discussion and Conclusion

In this paper, we have proposed a plasma simulation package JefiPIC, which solves the challenging task of describing plasma systems in terms of a 3-D particle-in-cell method combined with the Jefimenko's equations on GPU. The particles are pushed by the traditional particle simulation method, and the

volume-weighted charge and field interpolation methods are employed. Because the locations to allocate fields, charge density and current density are changed from the FDTD to Jefimenko's equations, we have modified the interpolation method accordingly. Through the comparisons with the results from EPOCH and RGB-Maxwell, we verify the credibility of JefiPIC. Our first-order accurate PIC code has the similar results as the second-order accurate Boltzmann equations, and shows a better solution of the electrostatic problem compared with results solved by the difference equations. Meanwhile, the time cost of JefiPIC is acceptable in dealing with the plasma problem. Our code has a benefit in describing plasma systems with open boundary conditions.

Though, JefiPIC in this version can only solve the collisionless Vlasov equations, the interactions between electrons and neutral molecules or charged ions need to be added to make the code more widely applicable.

Acknowledgement

We thank Prof. J. Wang for the helpful discussions on the PIC simulations. The work is supported by the National Natural Science Foundation of China (NSFC) under Grants No. 12105227.

Reference

- [1]. J. Dawson, One-dimensional plasma model, *The Physics of Fluids*, 5(4) (Apr.1962) pp. 445-459 doi: 10.1063/1.1706638.
- [2]. A. B. Langdon and C. K. Birdsall, Theory of plasma simulation using finite-size particles, *The Physics of Fluids*, 13(8) (Aug. 1970) pp. 2115-2122 doi: 10.1063/1.1693209.
- [3]. C. K. Birdsall and D. Fuss, Clods-in-clouds, clouds-in-cells physics for many-body plasma simulation, *Journal of Computational Physics*, 3(4) (Apr. 1969) pp. 494-511, doi: 10.1016/0021-9991(69)90058-8.
- [4]. B. Marder, A method for incorporating Gauss' law into electromagnetic PIC codes, *Journal of Computational Physics*, 68(1) (Jan. 1987) pp. 48-55 doi: /10.1016/0021-9991(87)90043-X.
- [5]. J. Villasenor, O. Buneman, Rigorous charge conservation for local electromagnetic field solvers, *Computer Physics Communications*, 69(2-3) (Mar.-Apr. 1992) pp. 306-316 doi: 10.1016/0010-4655(92)90169-Y.
- [6]. C. K. Birdsall, Particle-in-cell charged-particle simulations, plus Monte Carlo collisions with neutral atoms, *PIC-MCC*, *IEEE Transactions on Plasma Science*, 19(2) (Apr. 1991) pp. 65-85 doi: 10.1109/27.106800.
- [7]. V. Vahedi, M. Surendra, A Monte Carlo collision model for the particle-in-cell method: applications to argon and oxygen discharges, *Computer Physics Communications*, 87(1-2) (May 1995) pp. 179-198 doi: 10.1016/0010-4655(94)00171-W.
- [8]. B. Wang, et al., Modern gyrokinetic particle-in-cell simulation of fusion plasmas on top supercomputers, *The International Journal of High Performance Computing Applications*, 33(1) (Jan. 2019) pp. 168-188 doi: 10.1177/11094342017712059.
- [9]. T. D. Arber, et al., Contemporary particle-in-cell approach to laser-plasma modelling, *Plasma Physics and Controlled Fusion*, 57(11) Article. 113001 (Sept. 2015) doi: 10.1088/0741-3335/57/11/113001.
- [10].J. Chen and J Zhang, Impact of geometrical parameters on SGEMP responses in cylinder model, *Nuclear Engineering and Technology*, 54(9) (Sept., 2022) pp. 3415-3421 doi: 10.1016/j.net.2022.04.018.
- [11].H. Zhang, et al. Particle-in-cell simulations of low-pressure air plasma generated by pulsed x rays, *Journal of Applied Physics*, 130(17) Article. 173303 (Nov. 2021) doi:10.1063/5.0057841.
- [12].Z. Xu, et al., A code verification for the cavity SGEMP simulation code LASER-SGEMP, *IEEE Transactions on Nuclear Science*, 68(6) (Jun. 2021) pp. 1251-1257 doi: 10.1109/TNS.2021.3078739.
- [13].Q. Lu, et al., Particle-in-cell simulations of whistler waves excited by an electron K distribution in space plasma, *Journal of Geophysical Research Space Physics*, 115 Article. A02213 (Feb. 2010) doi:

10.1029/2009JA014580.

- [14].J. Chen, et al., 2D planar PIC simulation of space charge limited current with geometrical parameters, varying temporal-profile and initial velocities, *IEEE ACCESS*, 10 (2022) pp. 28499-28508 doi: 10.1109/ACCESS.2022.3158747.
- [15].J. Wang, A megawatt-level surface wave oscillator in Y-band with larger oversized structure driven by annular relativistic electron beam, *Scientific Reports*, 8 Article. 6978 (May 2018) doi: 10.1038/s41598-018-25466-w
- [16].D. R. Welch, Fast hybrid particle-in-cell technique for pulsed-power accelerators, *Physical review accelerators and beams*, 23(11) Article. 110401 (Nov. 2020) doi: 10.1103/PhysResAccelBeam.23.110401.
- [17].B. Goplen, et al., User-configurable MAGIC for electromagnetic PIC calculations, *Computer Physics Communications*, 87(1-2) (May 1995) pp. 54-86 doi: 10.1016/0010-4655(95)00010-D.
- [18].J. P. Verboncoeur, et al., An object-oriented electromagnetic PIC code, *Computer Physics Communications*, 87(1-2) (May 1995) pp. 199-211 doi: 10.1016/0010-4655(94)00173-Y.
- [19].J. D. Blahovec, et al., 3-D ICEPIC simulations of the relativistic klystron oscillator, *IEEE Transactions on Plasma Science*, 28(3) (June 2000) pp. 821-829 doi: 10.1109/27.887733.
- [20].J. Wang, et al., UNIPIC code for simulations of high power microwave devices, *Phys. Plasmas*, 16(3) (Mar. 2009) Article. 033108 doi:10.1063/1.3091931.
- [21].T. D. Arber, et al., Contemporary particle-in-cell approach to laser-plasma modelling, *Plasma Physics and Controlled Fusion*, 57(11) Article. 113001 (Sept. 2015) doi: 10.1088/0741-3335/57/11/113001.
- [22].C. P. Ridgers, et al., Modelling gamma-ray photon emission and pair production in high-intensity laser-matter interactions, *Journal of Computational Physics*, 260(1) (Mar. 2014) pp. 273-285 doi: 10.1016/j.jcp.2013.12.007.
- [23].K. Yee, Numerical solution of initial boundary value problems involving maxwell's equations in isotropic media, *IEEE Transactions on Antennas and Propagation*, 14(3) (May 1966) pp. 302-307 doi: 10.1109/TAP.1966.1138693.
- [24].D-Y. Na, Y. A. Omelchenko, H. Moon, B. V. Borges, F. L. Teixeira, Axisymmetric Charge-Conservative Electromagnetic Particle Simulation Algorithm on Unstructured Grids: Application to Microwave Vacuum Electronic Devices, *Journal of Computational Physics*, 346 (Oct. 2017) pp. 295-317 doi: 10.1016/j.jcp.2017.06.016.
- [25].D.-Y. Na, H. Moon, Y. A. Omelchenko, and F. L. Teixeira, Relativistic extension of a charge-conservative finite element solver for time-dependent Maxwell-Vlasov equations, *Physics of Plasmas*, 25(1) Article. 013109 (Jan. 2018) doi: 10.1063/1.5004557.
- [26].J. P. Verboncoeur, Symmetric Spline Weighting for Charge and Current Density in Particle Simulation, *Journal of Computational Physics*, 174(1) (Nov. 2001) pp. 421-427 doi: 10.1006/jcph.2001.6923.
- [27].T. Zh. Esirkepov, Exact charge conservation scheme for Particle-in-Cell simulation with an arbitrary form-factor, *Computer Physics Communications*, 135(2) (Apr. 2001) pp. 144-153 doi: 10.1016/S0010-4655(00)00228-9.
- [28].Y. Wang, et al., Charge conserving emission technique for three-dimensional conform particle-in-cell simulations, *High Power Laser and Particle Beams*, 28(3) (Mar. 2016) Article. 033020 doi: 10.11884/HPLPB201628.033020.
- [29].O. D. Jefimenko, Electricity and magnetism: an introduction to the theory of electric and magnetic fields, Electret Scientific Co, Star City, W. Va, 1989.
- [30].D. Griffiths, Introduction to electrodynamics, Prentice Hall, Upper Saddle River, N.J, 1999.
- [31].G. G. Howes, Laboratory space physics: Investigating the physics of space plasmas in the laboratory, 25(5) (Apr. 2018) Article. 055501 doi: 10.1063/1.5025421.
- [32].J. Zhang, et al., Charge-dependent directed flows in heavy-ion collisions by Boltzmann-Maxwell

equations, Physical Review Research, 4(3) (Aug. 2022) Article. 033138 doi: 10.1103/PhysRevResearch.4.033138.

[33].G. Peng, et al., Two typical collective behaviors of the heavy ions expanding in cold plasma with ambient magnetic field, Physics of Fluids, 33 Article. 076602 (Jul. 2021) doi: 10.1063/5.0053404

[34].S. H. Brecht and D. J. Larson, The physics of ion decoupling in magnetized plasma expansions, Journal of Geophysical Research: Space Physics, 116(A11) Article. A11310 (Nov. 2011) doi: 10.1029/2011JA016904.

[35].J. Chen, et al., Simulation of SGEMP using particle-in-cell method based on conformal technique, IEEE Transactions on Nuclear Science, 66(5) (May, 2019) pp. 820-826 doi:10.1109/TNS.2019.2911933.

[36].J. Berenger, A perfectly matched layer for the absorption of electromagnetic waves, Journal of Computational Physics, 114(2) (Oct. 1994) pp. 185-200 doi: 10.1006/jcph.1994.1159.

[37].G. Mur, Absorbing boundary conditions for the finite-difference approximation of the time-domain electromagnetic-field equations, IEEE Transactions on Electromagnetic Compatibility, EMC-23(4) (Nov. 1981) pp. 377-382 doi: 10.1109/TEMC.1981.303970.

[38].M. Gaffar and D. Jiao, On the low-frequency breakdown of FDTD, 2015 IEEE International Symposium on Antennas and Propagation & USNC/URSI National Radio Science Meeting, (2015) pp. 338-339 doi: 10.1109/APS.2015.7304555.

[39].K. Chen, et al., New Mixed SETD and FETD methods to overcome the low-frequency breakdown problems by tree-cotree splitting, IEEE Transactions on Microwave Theory and Techniques, 68(8) (Aug. 2020) pp. 3219-3228 doi: 10.1109/TMTT.2020.2995721.

[40].J. Zhang, et al., JefiGPU: Jefimenko's equations on GPU, Computer Physics Communications, 276 Article. 108328 (Jul. 2022) doi: 10.1016/j.cpc.2022.108328.

[41].H. Wu, et al., ZMCintegral: A package for multi-dimensional Monte Carlo integration on multi-GPUs, Computer Physics Communications, 248 Article. 106962 (Mar. 2020) doi: 10.1016/j.cpc.2019.106962.

[42].J. Zhang, et al., Towards a full solution of the relativistic Boltzmann equation for quark-gluon matter on GPUs, Physical Review D, 102(7) (Oct. 2020) Article. 074011 doi: 10.1103/PhysRevD.102.074011.

[43].R. Courant, K. Friedrichs and H. Lewy, On the partial difference equations of mathematical physics, IBM Journal of Research and Development, 11(2) (Mar. 1967) pp. 215-234 doi: 10.1147/rd.112.0215.

Appendix

Physical quantity	SI Unit	Flexible Unit
Magnetic field	T	$5.01398 \times 10^{-36} / (\lambda^2 \hbar^{3/2} \epsilon_0^{1/2} c^{5/2}) E^2$
Length	m	$3.16304 \times 10^{25} \hbar c \lambda E^{-1}$
Time	s	$9.48253 \times 10^{33} \hbar \lambda E^{-1}$
Electric charge	C	$1.89032 \times 10^{18} (\hbar \epsilon_0 c)^{1/2}$
Momentum	$\text{kg} \cdot \text{m} \cdot \text{s}^{-1}$	$2.99792 \times 10^8 / (c \lambda) E$
Energy	J	$1/\lambda E$
Mass	kg	$8.89752 \times 10^8 / (c^2 \lambda) E$
Electric current	A	$1.99347 \times 10^{-16} (\epsilon_0 c / \hbar)^{1/2} / \lambda E$
Electric field	$\text{V} \cdot \text{m}^{-1}$	$1.67249 \times 10^{-44} / (\lambda^2 \hbar^{3/2} \epsilon_0^{1/2} c^{3/2}) E^2$
Force	$\text{kg} \cdot \text{m} \cdot \text{s}^{-2}$	$3.16153 \times 10^{-26} / (\hbar \epsilon_0 c) E^2$
Unit charge	1	$0.30286 (\hbar \epsilon_0 c)^{1/2}$

In Flexible Unit (FU), all physical quantities have the dimension of energy E. One needs to **choose proper**

values for λ , c , $h\hbar$, ϵ_0 so that all numerical quantities are in the range of float64 on GPU, where c , \hbar , ϵ_0 denote the speed of light, the reduced Planck constant, and the vacuum permittivity. λ is constant relating the energy quantity between SI and FU.